

Nucleation, growth, and linkage of faults in oblique rift zones: Results from experimental clay models and implications for maximum fault size

Amy E. Clifton Nordic Volcanological Institute, 108 Reykjavík, Iceland

Roy W. Schlische Department of Geological Sciences, Rutgers University, Piscataway, New Jersey 08854-8066, USA

ABSTRACT

We use scaled clay models to study the temporal evolution of fault populations in experiments of moderately oblique ($\alpha = 60^\circ$) and highly oblique ($\alpha = 30^\circ$) distributed extension, where α is the angle between the rift axis and the direction of displacement. Faults nucleate at random heterogeneities, enhancing nucleation of diffuse clusters of new faults. In the highly oblique model, clusters of displacement-normal faults form parallel arrays, leading to fault growth dominated by tip propagation and along-strike linkage until maximum length is achieved. Subsequent growth of rift-subparallel faults leads to a phase of growth characterized by linkage and formation of branching faults. In the moderately oblique model, clusters form in a stepping geometry, leading to growth dominated by linkage. Faults nucleate and grow more rapidly, and their growth is less restricted than in the highly oblique model. Our results have implications for the maximum size earthquake to be expected in an oblique rift setting.

Keywords: oblique rifting, fault growth, experimental modeling, earthquakes, extensional tectonics.

INTRODUCTION

Scaled experimental models are useful for studying the evolution of geologic systems, because their boundary conditions are known. Scaled models can show nucleation, growth, and interaction of faults as their population evolves. Analyses of models can guide and support investigations in natural settings and have immediate relevance for earthquake hazard assessment, understanding fault sealing, fluid flow, and depositional patterns.

We examine the effect of rift obliquity on the evolution of fault populations and the potential size and distribution of earthquakes in extensional settings. Rift obliquity is related to the angle, α , between the rift trend and the direction of displacement of the rift walls (Withjack and Jamison, 1986), so that α is inversely related to the degree of obliquity. Work in oblique rift zones (e.g., Umhoefer and Stone, 1996; Chorowicz and Sorlein, 1992; Dauteuil and Brun, 1996; Applegate and Shor, 1994) as well as scaled modeling experiments (e.g., Withjack and Jamison, 1986; Tron and Brun, 1991; McClay and White, 1995; Clifton et al., 2000) have shown how rift obliquity affects fault geometry and spatial distribution. However, little is known about what role it plays in the temporal evolution of fault populations. We examine how fault nucleation, growth, and interaction vary with α by comparing modeling results from a moderately oblique ($\alpha = 60^\circ$) and a highly oblique rift ($\alpha = 30^\circ$). We discuss the implications of our

results for earthquake hazard assessment in oblique rift zones.

EXPERIMENTAL APPROACH

The experimental technique, scaling, and apparatus used in this study were fully described in Clifton et al. (2000). Models were subjected to different combinations of extension and shear by changing the orientation of a metal base plate attached to a moving wall (Fig. 1). A 6-cm-wide latex sheet was taped to straddle the metal base plate and a stationary plate beneath it. As the moving wall was displaced at a constant rate of 3 cm/h, a 2.5-cm-thick layer of wet clay underwent distributed deformation above the uniformly stretching latex sheet. Our models represent distributed deformation of a brittle layer above a narrow zone that deforms continuously. Thus, this approach is best suited to modeling oblique oceanic spreading centers and continental rift systems that have localized in regions where the crust is weaker than surrounding areas. The major difference between geology and the models is that some natural faults may be reactivated faults, whereas there are no reactivated faults in the model. To record the temporal evolution of the fault population, photographs were taken after every 0.25 cm of displacement of the moving wall. Scanned photographs were used to prepare fault trace maps consisting of polygons drawn around the horizontal projections of hanging-wall and footwall cutoffs on the top surface of the clay. Fault trace maps for one increment

were overlain on images of the next to correctly position the study area boundaries and to ensure consistency in identifying faults. Images analyzed here were taken between 1 cm and 3.5 cm of displacement. Data consist of the number of visible faults, their trend, and tip to tip length. Terms used to describe the models are defined as follows. A rift zone is the area directly above the latex sheet. A deforming zone includes the entire faulted area. A rift margin is the zone of faulting outboard of the latex sheet.

FAULT POPULATION EVOLUTION IN OBLIQUE RIFT ZONES

Moderately Oblique Rift, $\alpha = 60^\circ$

For the $\alpha = 60^\circ$ experiment (Fig. 2), faults nucleate around random flaws (e.g., small air bubbles) in the clay. The first faults appear in the rift zone and are relatively straight, isolated structures. As extension continues, new faults tend to nucleate close to these first faults, forming diffuse clusters in the center of the rift. At 2.0 cm of displacement, faults appear at the rift margin closest to the moving wall. In general, faults dip inward toward the center of the rift zone, which is the area of maximum thinning and subsidence of the clay. After 2.5 cm of displacement, the number of nucleating faults within the rift zone decreases dramatically; deformation is dominated by faults that lengthen along strike, gain displacement, and link with other faults. Fault nucleation also decreases along the rift margin closest to the moving wall. However, faults first appear on the margin farthest from the moving wall at 2.75 cm of displacement. New faults continue to nucleate along both margins as older faults lengthen. At 3.5 cm of displacement, the rift margin closest to the moving wall is characterized by long, relatively straight faults with a rift-parallel trend. Faults on the opposite margin are shorter and strike oblique to the trend of the rift zone, but form an en echelon array that is rift parallel.

Histograms of azimuths for the $\alpha = 60^\circ$ model (Fig. 3) show that although most of the earliest faults have a trend that is perpendicular to the direction of regional extension (i.e., displacement normal), many faults are oblique to that trend. Almost from the beginning, the histogram is skewed toward the rift trend, and

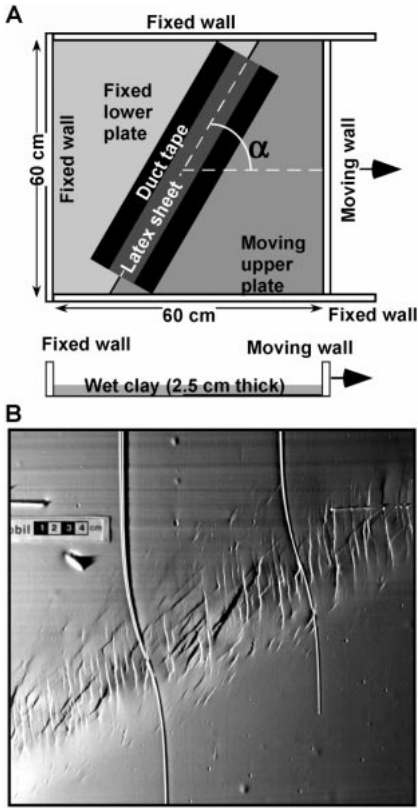


Figure 1. A: Detail of experimental apparatus in map view without clay layer, showing that α is defined as acute angle between rift axis and displacement direction (Withjack and Jamison, 1986) and with clay layer in cross section. **B:** Photo of $\alpha = 30^\circ$ model after 2.5 cm of displacement. Thick vertical lines are trowel marks on model surface.

this skewness becomes more pronounced as extension proceeds. Early in the model run, the histogram peak becomes oblique to the displacement-normal trend. Plots of length versus azimuth (triangles in Fig. 3) show that most rift-subparallel faults are short, whereas the longest faults strike oblique to the displacement-normal direction. The appearance of more rift-subparallel faults at 2.5 cm of displacement is a result of continued fault nucleation at the rift margins (see preceding).

Highly Oblique Rift, $\alpha = 30^\circ$

In the $\alpha = 30^\circ$ experiment (Fig. 4), faults first appear at 1.5 cm of displacement. From the start, two sets of faults are evident. One has a displacement-normal strike with right-lateral oblique slip. The other has a rift-subparallel strike with left-lateral oblique slip. These faults are relatively straight and have subvertical dips, initially showing only a small component of dip slip. The zone of deformation starts out wider than the latex sheet, and faults are uniformly distributed across the width of the deformed zone.

At 2.0 cm displacement, faults at the rift

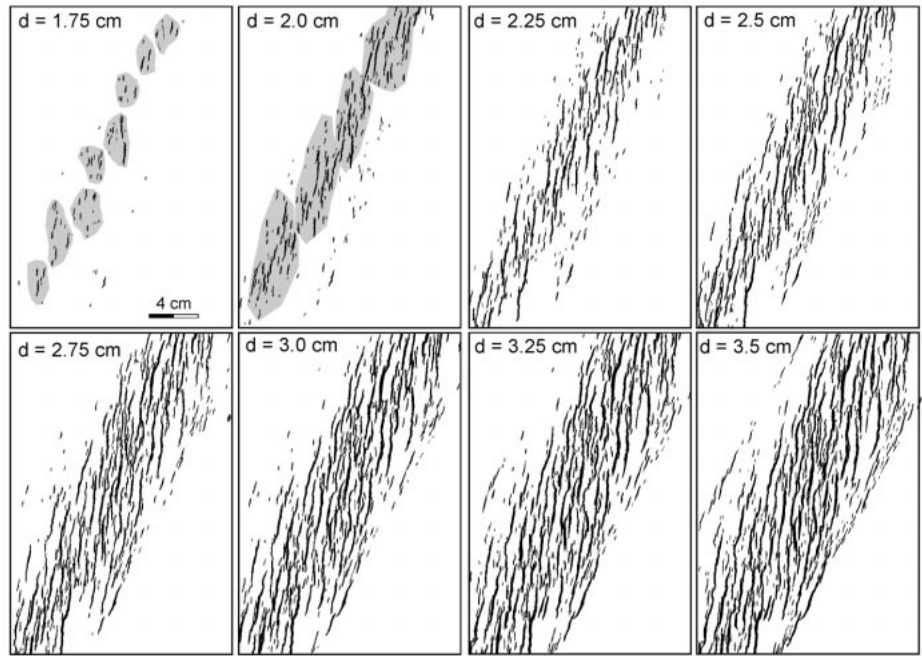


Figure 2. Fault trace maps for $\alpha = 60^\circ$ between 1.75 and 3.5 cm of displacement (d). Moving wall is to right. Gray shading identifies fault clusters.

margin have a different strike than the majority of faults in the rift zone. All faults at the margin strike oblique to the rift-parallel trend, whereas the great majority of faults in the rift zone have a strike that is displacement normal. A subtle clustering of displacement-normal faults develops in the center of the deforma-

tion zone early in the model evolution. At 2.5 cm displacement, histograms of azimuth (Fig. 3) show an increase in the number of rift-subparallel faults and, at 3.5 cm displacement, they are more numerous than displacement-normal faults. Most rift-subparallel faults form along the rift margins; however, at 2.5 cm dis-

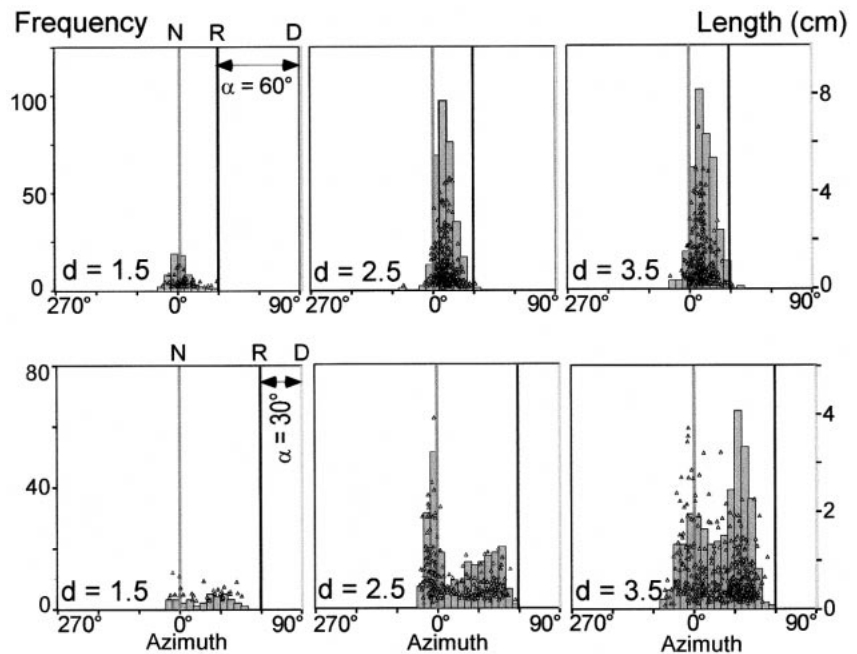


Figure 3. Graphs showing histograms of azimuth (patterned bars) and length vs. azimuth (triangles) for $\alpha = 60^\circ$ and $\alpha = 30^\circ$ models at 1.5, 2.5, and 3.5 cm displacement (d) increments. N = displacement-normal direction; R = rift trend; D = displacement direction. Note that displacement-normal peak in $\alpha = 30^\circ$ model decreases between 2.5 and 3.5 cm of displacement due to linkage of two fault sets through time.

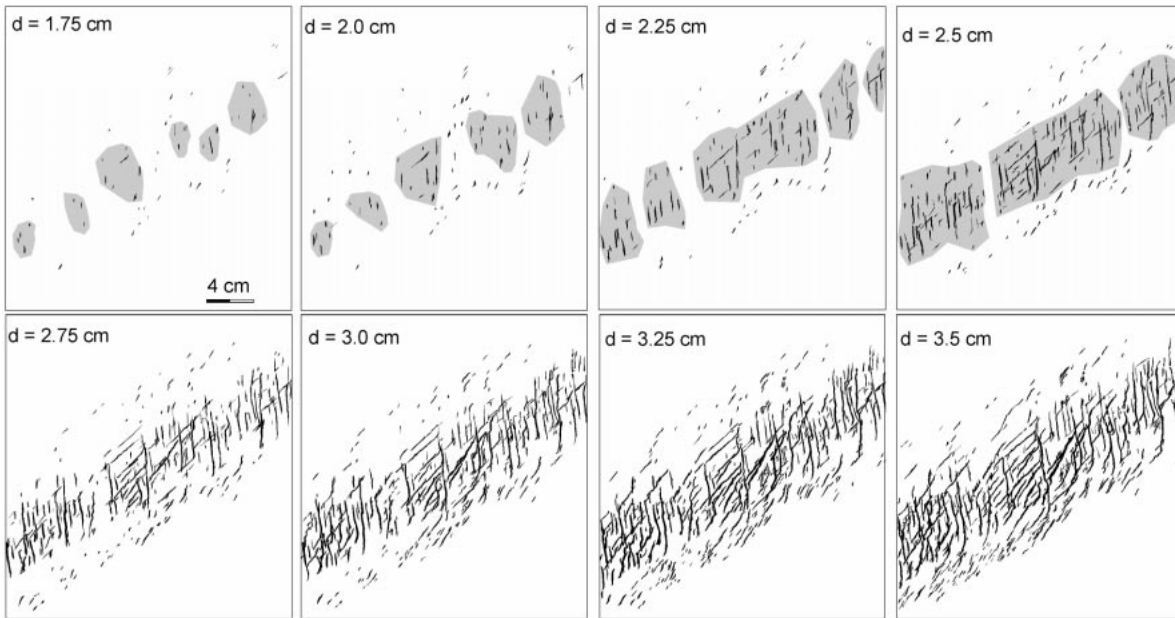


Figure 4. Fault trace maps for $\alpha = 30^\circ$ between 1.75 and 3.5 cm of displacement (d). Moving wall is to right. Gray shading identifies fault clusters.

placement, many are also present in the rift zone. At first they tend to be short, isolated structures that fill the spaces between displacement-normal faults. As their number increases, they begin to interact with displacement-normal faults, forming complex, anastomosing or branching structures. During linkage, some rotate into an orientation that is perpendicular to the direction of maximum horizontal extension (E_{hmax}). Once in this orientation, they gain displacement rapidly. Plots of length versus azimuth (triangles in Fig. 3) reflect this interaction of the two fault sets. Faults with a strike intermediate between rift parallel and displacement normal increase both in number and length as a result of linkage between these two subpopulations.

Faults on the rift margin closest to the moving wall develop first. They continue to nucleate throughout the model run and retain an average strike that is 20° oblique to the rift trend. Most faults on the rift margin grow by tip propagation rather than linkage, so that faults here remain relatively short compared to those within the rift zone.

DISCUSSION

Fault Nucleation

In both models, the number of faults generally increases with increasing displacement of the moving wall (Fig. 5A). However, the rate of increase for the $\alpha = 60^\circ$ model is more variable than for the $\alpha = 30^\circ$ model. After 1.75 cm of displacement, the number of faults increases by 300% in the $\alpha = 60^\circ$ model. Subsequently, the rate of nucleation decreases, and, at 2.5 cm of displacement, levels off. This reflects a significant fault linkage event

(see following). An increase in fault nucleation after 3.0 cm of displacement is confined to the rift margins. The number of faults on the $\alpha = 30^\circ$ model increases steadily through time, with the exception of a $>100\%$ increase between 2.25 and 2.5 cm of displacement. Subsequently, faults continue to nucleate at a steady rate, although increasingly more nucleation occurs on the rift margins.

Fault Growth

The rate of fault growth is reflected by the summed length (ΣL) of faults normalized to the area of the deformed zone (Fig. 5B) and changes in the length of faults at the 95th percentile of length for all faults in the model (L_{95} ; Fig. 5C). Until 1.75 cm of displacement, ΣL and L_{95} are approximately equal for both models. As extension proceeds, the rate of fault growth in both models becomes more rapid, perhaps indicating that a critical strain threshold is reached. This increase begins sooner and occurs at a higher rate in the $\alpha = 60^\circ$ model. ΣL and L_{95} for this model follow a more or less parallel trend of steady increase.

For the $\alpha = 30^\circ$ model, ΣL increases steadily throughout the model run, but L_{95} approaches its maximum value after only 2.5 cm of displacement. The angle of rift obliquity constrains the maximum length that faults can attain within the rift zone (Clifton et al., 2000). In the early stages of evolution of the $\alpha = 30^\circ$ model, faults with a displacement-normal trend cluster in parallel arrays. These become the longest faults on the model, but their growth is limited by the width of the rift zone. They can only become slightly longer

than this width. These displacement-normal faults grow by tip propagation and along-strike linkage until, at 2.5 cm displacement, they reach the edge of the rift zone, where further growth is inhibited. It is only at this point that rift-parallel faults start to increase rapidly in number. The length of these faults is in turn limited by the presence of long displacement-normal faults that span the width of the rift. Rift-parallel faults fill the gaps between clusters of displacement-normal faults and commonly terminate against them. In many cases, the two sets link to form complex, branching structures (Fig. 6). The tip to tip lengths of these complex faults are considerably shorter than their trace lengths, placing another constraint on maximum fault length.

Fault growth in the $\alpha = 60^\circ$ model is much less restricted. Until 1.75 cm displacement, growth is accomplished by tip propagation of small faults. Because the faults in this model form diffuse clusters, they do not have to attain a very great length before linkage can begin. Through most of the model's evolution, growth is accomplished primarily by linkage of faults arranged in an echelon or relay geometry (Fig. 6). Faults that nucleate in parallel arrays grow mainly by tip propagation and tend to remain relatively short. Fault geometry is such that the maximum attainable fault length is more than three times the width of the rift zone. At 2.5 cm displacement, deformation becomes concentrated on these long faults, and nucleation of new faults is inhibited.

The results presented here suggest that fault interaction begins at the earliest stages of fault population evolution, when the presence of

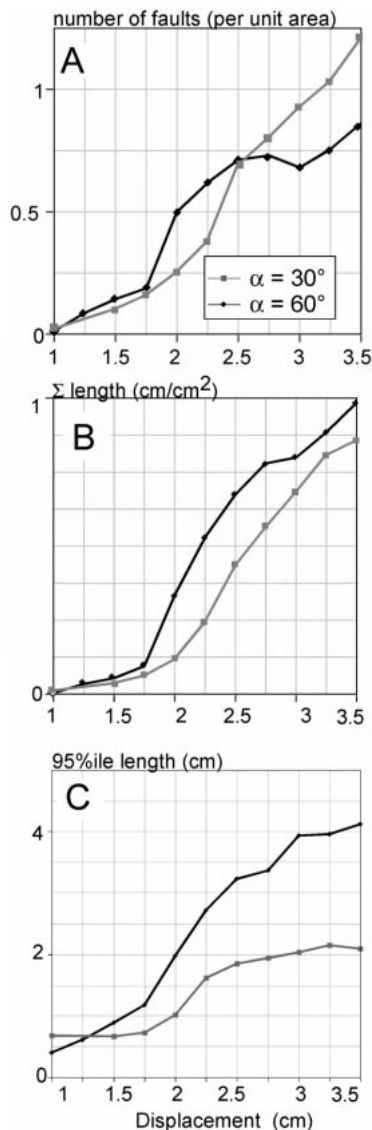


Figure 5. Summary plots of all data for $\alpha = 60^\circ$ and $\alpha = 30^\circ$ models showing how (A) number of faults (normalized by map area), (B) summed fault length (normalized by map area), and (C) 95th percentile of lengths change with increasing displacement on each model.

the first faults appears to enhance nucleation of nearby faults. This effect is more pronounced and occurs sooner in the less oblique $\alpha = 60^\circ$ model. Once diffuse clusters of small faults have formed in this model, their growth proceeds in a manner similar to that described for orthogonal rifts (e.g., Aydin and Schultz, 1990; Peacock and Sanderson, 1991; Trudgill and Cartwright, 1994). Fault tip zones interact via relay structures in the clay, and in most cases ramp breach is accomplished by the tip of one segment curving into either the hanging wall or footwall of the other. Clusters of parallel faults form on the $\alpha = 30^\circ$ model after

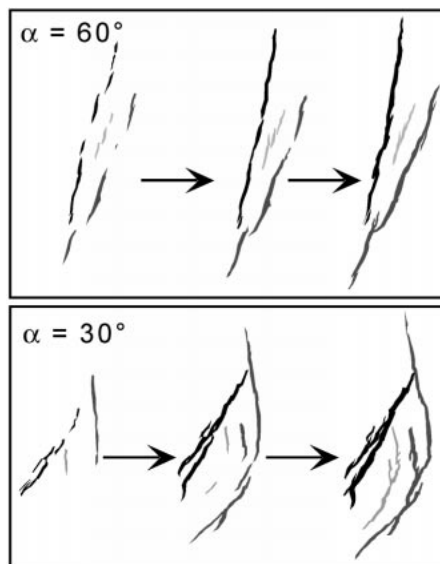


Figure 6. Detail of fault growth in $\alpha = 60^\circ$, and $\alpha = 30^\circ$ rift zones showing how faults link through time. Fault segments that will eventually link are shown with same gray or black tone.

~ 2.0 cm displacement. According to fault growth models (e.g., Trudgill and Cartwright, 1994; Gupta and Scholz, 2000), either they should not form or their growth should be limited by the high percentage of overlap. However, in our models these groups of parallel faults lengthen until their growth is stopped only when they reach the rift margin. Results of three-dimensional boundary element modeling (Willemse, 1997) suggest that overlapping faults can continue to grow if their down-dip height is small relative to their lengths. In the $\alpha = 30^\circ$ model, maximum down-dip height is only 25% of maximum fault length.

Our results demonstrate that there is a geometric upper limit to fault length in oblique rift zones. This has implications for earthquake hazard assessment in places such as Iceland, where all segments of the plate boundary are oblique to the spreading direction (Clifton et al., 2000). Assuming that potential earthquake hazard is related to fault length, then the maximum potential earthquake in a mature highly oblique rift should be less than that in an orthogonal or less oblique rift. Our results suggest that earthquakes on the margins of oblique rift zones should occur on faults with a rift-subparallel rather than a displacement-normal trend. However, in highly oblique rift zones such as Reykjanes Peninsula in Iceland, these earthquakes are likely to be small and pose less of a hazard than events on faults in the center of the rift. Earthquake activity in highly oblique rift zones may occur alternately on either displacement-normal or rift-subpar-

allel faults, and may occur on faults of both trends during the same event.

ACKNOWLEDGMENTS

This work was supported by Rutgers University, Mobil Technology Company, National Science Foundation grant EAR-9706199, and student research grants from the Geological Society of America, American Association of Petroleum Geologists, and Sigma Xi. We thank Martha Withjack for significant discussion and help in the laboratory and Nancye Dawers and Bruno Vendeville for reviews.

REFERENCES CITED

- Applegate, B., and Shor, A.N., 1994, The northern Mid-Atlantic and Reykjanes Ridges: Spreading center morphology between $55^\circ 50'N$ and $63^\circ 00'N$: *Journal of Geophysical Research*, v. 99, p. 17 935–17 956.
- Aydin, A., and Schultz, R.A., 1990, Effect of mechanical interaction on the development of strike-slip faults with echelon patterns: *Journal of Structural Geology*, v. 12, p. 123–129.
- Chorowicz, J., and Sorlien, C., 1992, Oblique extensional tectonics in the Malawi Rift, Africa: *Geological Society of America Bulletin*, v. 104, p. 1015–1023.
- Clifton, A.E., Schlichte, R.W., Withjack, M.O., and Ackermann, R.V., 2000, Influence of rift obliquity on fault-population systematics: Results of experimental clay models: *Journal of Structural Geology*, v. 22, p. 1491–1509.
- Dauteuil, O., and Brun, J.-P., 1996, Deformation partitioning in a slow spreading ridge undergoing oblique extension: Mohns Ridge, Norwegian Sea: *Tectonics*, v. 15, p. 870–884.
- Gupta, A., and Scholz, C.H., 2000, A model of normal fault interaction based on observations and theory: *Journal of Structural Geology*, v. 22, p. 865–879.
- McClay, K.R., and White, M.J., 1995, Analogue modelling of orthogonal and oblique rifting: *Marine and Petroleum Geology*, v. 12, p. 147–151.
- Peacock, D.C.P., and Sanderson, D.J., 1991, Displacements, segment linkage and relay ramps in normal fault zones: *Journal of Structural Geology*, v. 13, p. 721–733.
- Tron, V., and Brun, J.-P., 1991, Experiments on oblique rifting in brittle-ductile systems: *Tectonophysics*, v. 188, p. 71–84.
- Trudgill, B., and Cartwright, J., 1994, Relay ramp morphologies and normal fault linkages, Canyonlands National Park, Utah: *Geological Society of America Bulletin*, v. 106, p. 1143–1157.
- Umhoefer, P.J., and Stone, K.A., 1996, Description and kinematics of the SE Loreto basin fault array, Baja California Sur, Mexico: A positive field test of oblique-rift models: *Journal of Structural Geology*, v. 18, p. 595–614.
- Willemse, E.J.M., 1997, Segmented normal faults: Correspondence between three-dimensional mechanical models and field data: *Journal of Geophysical Research*, v. 102, p. 675–692.
- Withjack, M.O., and Jamison, W.R., 1986, Deformation produced by oblique rifting: *Tectonophysics*, v. 126, p. 99–124.

Manuscript received August 22, 2000
Revised manuscript received January 25, 2001
Manuscript accepted January 30, 2001

Printed in USA